

Static compression of LiH to 250 GPaA. Lazicki,^{1,*} P. Loubeyre,¹ F. Occelli,¹ Russell J. Hemley,² and M. Mezouar³¹*Département de Physique Théorique et Appliquée, CEA/DAM/DIF, F-91680 Bruyères-le-Châtel, France*²*Geophysical Laboratory, Carnegie Institution of Washington, Washington DC 20008, USA*³*ESRF, F-31800 Grenoble, France*

(Received 28 September 2011; revised manuscript received 11 January 2012; published 6 February 2012)

The equation of state of LiH was extended to 252 GPa ($V/V_0 = 32\%$) at room temperature using x-ray diffraction in diamond-anvil cells. LiH was shown to remain in the the NaCl ($B1$) structure under these conditions, and the predicted $B1$ - $B2$ phase transition well known in neighboring alkali halides was not observed. Raman spectroscopy performed up to 120 GPa revealed all transverse and acoustic phonon modes at the X point of reciprocal space. The structural, equation of state and thermodynamic properties clarified in this study enable the benchmarking of current theoretical models.

DOI: [10.1103/PhysRevB.85.054103](https://doi.org/10.1103/PhysRevB.85.054103)

PACS number(s): 64.30.-t, 62.50.-p

I. INTRODUCTION

Lithium hydride is the archetypal textbook example of a simple ionic compound. Its high-pressure properties are expected to be quite interesting because of the quantum influence of the protons and of the growing interaction of core electrons. Zero-point motion of hydrogen has been observed to give a measurable isotopic shift to its equation of state.¹ At compressions where core electron densities on neighboring atoms begin to overlap, unexpected and exotic behavior may be expected, such as the transitions to low-symmetry and electrone phases, room-temperature melting, and metal-insulator transitions, which have recently been observed in the lightweight alkali metals.²⁻⁵ LiH has a $B1$ structure at ambient temperature and pressure and maintains this phase up to at least 36 GPa (96 GPa for LiD), the highest pressures at which it has been examined experimentally so far.¹ The heavier alkali hydrides all undergo a $B1$ - $B2$ transition under pressure, and many computational efforts have attempted to predict when such a transition might be seen in LiH.⁶⁻¹³

The effects of pressure on the electronic properties of LiH are of interest, in part due to possible parallels with metallic hydrogen. The two monovalent elements have some similarities at extreme densities: metallic atomic hydrogen has been predicted to adopt lithium-like phases at high pressure,¹⁴ while dense lithium has recently been shown to have trends in high-pressure melting similar to the long-predicted metallic-liquid ground-state in hydrogen.¹⁵ Alternatively, Li could be viewed as an “impurity” in a hydrogen lattice, stabilizing forms of hydrogen bonding that otherwise would not arise until much higher pressure.¹⁶ At ambient conditions the electronic band gap of LiH is a moderate 4.9 eV, and it decreases steadily under pressure.¹⁷ Calculations have suggested that, while pressure-induced electronic gap closure may occur at pressures out of reach for static experimental methods, the predicted $B2$ phase will metallize at lower pressure, and it should be metallic at the predicted phase-transition pressure.¹² Various theoretical models have made predictions for this transition between 220 and 400 GPa,⁷⁻¹³ pressures that are attainable in diamond-anvil cells. The possibility of metallization in other stoichiometries of Li-H compounds has been examined theoretically as well, revealing several compounds in which electron transport from the electropositive Li ion results in

metallization of the hydrogen lattice at high pressure.¹⁶ Others have predicted superconductivity in the metallic phase of LiH.¹⁸

The ability of a theoretical model to accurately predict experimental volumes and compressibility and observables such as phase transitions or metallization is a very good test of its physical accuracy, particularly for such a compound where quantum effects and core interactions are not negligible. Thus far, however, experimental results are confined to pressures too low to really differentiate between theoretical models. We have therefore undertaken to extend experimental results into the multimegabar pressure regime, using x-ray diffraction to better constrain the experimental equation of state and to search for high-pressure structural or electronic phase transitions.

Vibrational properties have also been examined using Raman spectroscopy. Knowledge of the phonon modes under pressure can help constrain models for the zero-point energy, which has been shown to be important for predicting properties of LiH. Also, softening of phonon modes under pressure often signals structural instabilities that precede phase transitions. In the case of the alkali halides, it has been predicted that a softening of the transverse-acoustic (TA) phonon mode at the zone boundary X point will accompany the $B1$ - $B2$ transition.¹¹

II. EXPERIMENTAL METHODS

We have achieved pressure in excess of 250 GPa by compressing LiH in diamond-anvil cells with diamond-culet sizes ranging from 25 to 50 μm . Samples of high-purity LiH were handled in an inert argon or helium environment with less than 15 ppm oxygen and water. To maximize sample volumes (necessary because of the weakness of x-ray scattering from this compound) we have not used a pressure medium in most cases. This also minimizes the possibility of further contamination or chemical reaction in the sample. Two of the samples were loaded together with hydrogen to test for chemical reactions at high pressure to the predicted metallic H-rich stoichiometries.¹⁶ Careful observation of x-ray diffraction and Raman spectroscopy revealed no chemistry below 120 GPa, and so these data sets were included in the equation-of-state and Raman measurements reported here.

Formation of new Li-H compounds from compression of metallic lithium loaded in a H_2 medium was also attempted. When compressed at ambient temperature, stoichiometric LiH is invariably formed by 10 GPa. Immediate reaction was avoided by compressing Li in H_2 at low temperature (~ 94 K). Slow warming of the mixture at 80 GPa resulted again in the formation of stoichiometric LiH. Raman spectroscopy data from these investigations were also therefore included in this study. A more complete report of the chemistry study will be presented in a future presentation.

Pressure was determined either from the equation of state of micron-sized grains of gold¹⁹ placed in the sample chamber (for diffraction studies) or the calibrated pressure-induced shift of fluorescence from ruby²⁰ (for Raman studies). Samples were contained in rhenium gaskets. Based on the types of failures that led to diamond breakage at high pressure, it appears that LiH may chemically attack the rhenium, so most gaskets have been prepared with an ~ 0.5 - μm -thick gold ring insert. In one case a 0.2 - μm gold layer was sputtered onto the gasket. One diffraction experiment was carried out at low temperatures of 10–13 K in a helium cryostat. The data presented here summarize the measurements made on 12 different samples.

Angle-dispersive x-ray diffraction was performed at sector ID27 of the European Synchrotron Radiation Facility (ESRF) with 0.3738 - \AA monochromatic x rays. Scattered x rays were collected and recorded on a MAR 345 image plate detector. Collection times were 2–3 min in most cases. Diffraction from many of the LiH samples was single-crystal-like, and so diamond cells were oscillated 2° – 6° during collection in order to integrate over the rocking curves of the reflections. The diffraction patterns from the image plates were analyzed using FIT2D. Raman spectroscopy was performed using laser wavelengths of 514 or 488 nm. Spectra were collected by a single-stage spectrograph with a multichannel CCD detector, using techniques described elsewhere.²¹

III. RESULTS

LiH has an extremely low electron density, and thus diffraction is very weak. The (111) and (200) diffraction peaks are sufficiently intense to be measurable above the background, but in most cases the lower-intensity (111) peak overlaps with diffraction from the rhenium gasket or the gold gasket lining, so volume is determined from the (200) peak position alone. Above 200 GPa the (111) peak is again visible, but its intensity does not sufficiently exceed that of the background for a very precise determination of the position. The (200) peak position is, however, sufficient for defining the lattice parameter. For a $B1$ - $B2$ phase transition (with negligible volume change), the $B1$ (200) peak would disappear, and the dominant $B2$ peak (110) would appear approximately between 1° and 2° in 2θ from the $B1$ (200) position. At the highest pressure achieved, the strongest $B2$ peaks would, in fact, be overlapping the gold diffraction peaks, so we cannot rule out the possibility that a small amount of $B2$ phase could be present together with the $B1$ (or the possibility of a different, as yet unpredicted, phase with weak or coincident peaks). Evolution of the (200) peak up to the highest pressure achieved in this study is shown in Fig. 1. The negligible peak broadening indicates

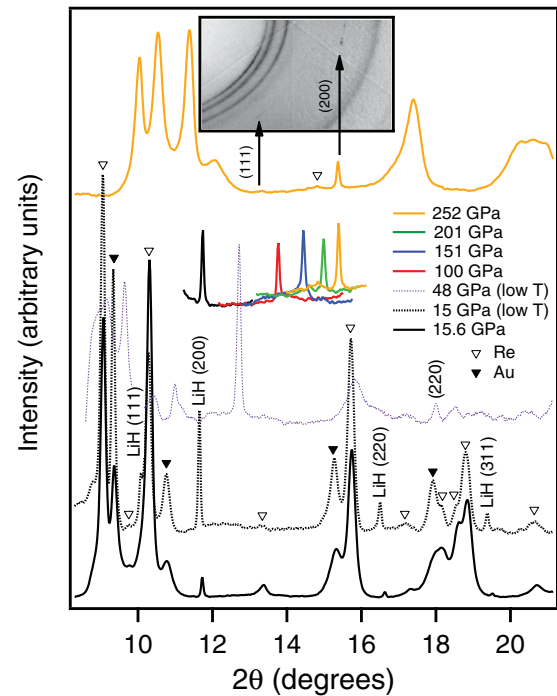


FIG. 1. (Color online) Integrated x-ray diffraction patterns at low pressure (~ 15 GPa) and at ambient and low temperature (11 K) showing scattering from LiH and from the Re gasket and the Au pressure calibrant. The (111), (200), (220), and (311) peaks of LiH are evident at low pressure. At ambient temperature all but the relatively much more intense (200) peak are lost or nearly lost at low pressure due to the rising background or overlap with Re and Au scattering. The pressure evolution of the (200) peak at ambient temperature is shown (vertical scaling expanded), demonstrating a lack of broadening. In the low-temperature study it is possible to track the (220) peak to higher pressures (shown, for example, at 48 GPa). The full diffraction pattern at the highest measured pressure (252 GPa) and ambient temperature is shown, together with a section of the raw image plate data.

that nonhydrostatic stresses in the cell are not significant. In the low-temperature study (where two peaks were evident up to the maximum pressure), we compare the LiH lattice parameters calculated from both the (200) and (220) peaks (Fig. 2). In other fcc crystals, the (200) peak position has been shown to be much more sensitive to uniaxial stress than the (220) peak if conditions are nonhydrostatic.^{22,23} In this

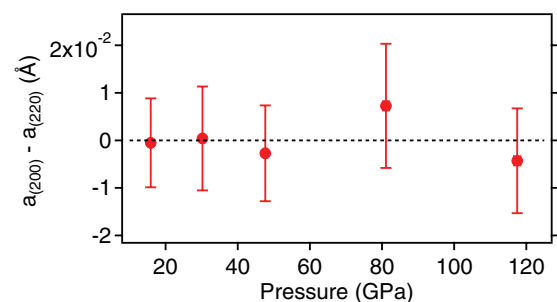


FIG. 2. (Color online) Difference between lattice parameters calculated using the (200) and (220) reflections from LiH in run 1.

case, the difference is unsystematic and very slight, smaller than experimental uncertainty, indicating that strain conditions in the sample chamber are essentially homogeneous, even at low temperature and in the absence of a pressure medium. The effects of nonhydrostatic conditions are generally a premature stiffening of the material, reflected by a higher bulk modulus, or stabilization of a particular phase beyond its region of energetic stability. Nonhydrostatic conditions generally cause a phase transition to occur at lower pressure, when the strain induced by the uniaxial compression favors a particular crystal deformation.^{25,26} We believe, based on the above-stated arguments as well as the good agreement between our equation-of-state measurements performed using no pressure medium compared to data collected under optimally hydrostatic conditions with a helium medium up to 36 GPa,¹ that the equation-of-state measurements made in this study are not strongly affected by nonhydrostatic effects.

LiH crystal structure was measured for eight different samples over a large pressure range. The compound is found to retain the *B1* phase up to at least 254 GPa (a volume reduction of 0.32). The fact that nonhydrostatic conditions generally lower the phase-transition pressure indicates that, in this study, we have certainly not entered the stability regime of the *B2* phase. Pressures were determined from the shift of the (111) peak of gold, which has been shown to be least sensitive to uniaxial strain. In the highest-pressure study (run 7), pressure was calibrated from the equation of state of the sputtered gold layer. Diffraction from the nanometer-scale layer revealed an unusual structural evolution, perhaps due to surface effects or high-strain conditions, leading to unexpected pressure values. To mitigate these effects we attempt to correct for uniaxial stresses using the formalism set out by Singh *et al.*,²⁴ using elastic constants from Ref. 27. The parameter α (notation from Ref. 24), which determines the uniaxial stress component, is not experimentally established but should lie between 0.5 and 1.0, with a value of 1.0 corresponding to least stressed states. We find that in order to bring the data from run 7 into reasonable agreement with the other experimental runs we must assume the other extreme of maximum uniaxial stresses ($\alpha = 0.5$). Because of the model dependence of these data, we do not use this run in our fitting of the equation of state. The same analysis was applied to the rest of the data, assuming a very low-stress condition, and it was found that correcting for nonhydrostatic effects with a value of $\alpha = 1$ results in equation-of-state fitting parameters that only differ from the uncorrected results [pressure calibrated purely from the position of the gold (111) peak] by $\sim 3\%$ or less, in most cases within the error bar on the measurement. As a result we prefer again to avoid the model-dependent result, and we quote pressure values taken simply from the Au (111) peak.

The Vinet equation,^{28,29}

$$P = 3K_0(1 - X)X^{-2} \exp[3/2(K'_0 - 1)(1 - X)], \quad (1)$$

with $X = (V/V_0)^{1/3}$, derived from an empirical potential and known to best describe experimental data at extreme pressures, is used to fit our data. The equation can be reformulated in terms of expressions analogous to normalized

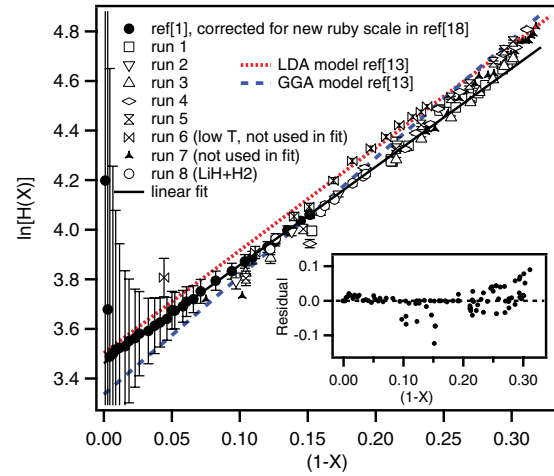


FIG. 3. (Color online) Normalized stress as a function of Eulerian strain with a linear fit to all data sets with the exception of run 6, which has a slight temperature shift, and run 7, for which the pressure measurement is uncertain, as described in the text. The inset shows residuals from linear fit, showing deviation above $(1 - X) \sim 0.28$.

stress, $\ln[H(X)] = \ln\left[\frac{PX^2}{3(1-X)}\right]$, and Eulerian strain, $(1 - X)$. This gives

$$\ln[H(X)] = \ln K_0 + \eta(1 - X), \quad (2)$$

with

$$\eta = \frac{3}{2}(K'_0 - 1). \quad (3)$$

In the absence of phase transitions, the data should follow a linear trend. It is evident from Eq. (2) that the slope yields the pressure derivative of the bulk modulus K'_0 . Such a treatment of our data from multiple experimental runs is shown in Fig. 3. $\ln[H(X)]$ has a high uncertainty as $(1 - X) \rightarrow 0$, and thus the data below $(1 - X) = 0.035$ are excluded from the fit. Constraining the value for K'_0 in this manner, we then fit the pressure as a function of relative volume with Eq. (1) to determine the bulk modulus K_0 . Fitting parameters are reported in Table I and compared to a variety of experimental and theoretical results. The Vinet $P(V)$ equation of state along with experimental data points is shown in Fig. 4. The fit reproduces the compression curve of LiH very well up to 200 GPa. Above this pressure, a difference in compressibility is observed.

LiH in the *B1* structure has no first-order Raman modes due to the inversion symmetry about every ion. Second-order Raman scattering, however, has been shown to give two-phonon features, which correspond to sum modes of zone-boundary phonons. Ho *et al.*³² have suggested assignments for experimentally observed modes up to 15 GPa. We extend the measured pressure range of several of the two-phonon modes to above 60 GPa and in one case up to 120 GPa (Fig. 5). Following the assignments of Ho *et al.*, we calculate combinations of the various two-phonon modes to extract all zone boundary phonons at the X point.

TABLE I. Equation-of-state fitting parameters and proposed $B1$ - $B2$ phase transition pressure (probably coincident with metallization) compared with previous experimental and theoretical results. Abbreviations used are as follows: LDA, local-density approximation; GGA, generalized gradient approximation; ZP, zero-point motion; Debye, Debye approximation for zero-point motion; QH, quasiharmonic approximation for zero-point motion.

	a_0 (Å)	K_0 (GPa)	K'_0	$B1$ - $B2$ transition (GPa)
Experiments				
This work (300 K)	4.080 (fixed)	33.1(3)	3.64(5)	>254 GPa ($0.32V_0$)
This work (10-15 K)	4.07(4)	35(3)	3.6(3)	
High-pressure diffraction ^a (Ref. 1)	4.080	31.9(1)	3.62(2)	
Ambient diffraction (Ref. 30)	4.084	33.6	4 (fixed)	
Ultrasonic pulse echo method (Ref. 31)	4.084 (fixed)	32.35	3.78	
Calculations				
LDA + ZP (Debye), 0 K (Refs. 7 and 8)	4.000	36.6	3.40	226 GPa ($0.37V_0$)
LDA + ZP (QH) (Ref. 9)	4.038	31	3.5	450–500 GPa ($0.25V_0$)
LDA + ZP (QH) (0 K) (Ref. 13)	3.992	35.8	3.51	308 GPa ($0.33V_0$)
LDA + ZP (QH) (300 K) (Ref. 13)	4.009	33.2	3.76	
GGA + ZP(QH) (0 K) (Ref. 13)	4.094	31.6	3.59	
GGA + ZP(QH) (300 K) (Ref. 13)	4.118	28.1	4.18	
GGA + ZP (QH from Ref. 10) (Ref. 12)	4.08	33.9		329 GPa ($0.29V_0$)

^aPressures corrected for updated ruby scale.²⁰

IV. DISCUSSION

Equation-of-state fitting parameters for LiH are shown in Table I, compared with published experimental and theoretical data. Our results are consistent with or slightly softer than other experimental results. Models most accurately predicting lattice parameters of LiH are those using the generalized gradient approximation (GGA) and including the quasiharmonic approximation for zero-point motion, such as those of Yu *et al.*¹³ Experimental results for the bulk modulus and its pressure derivative at low and ambient temperatures seem more consistent with the local-density approximation (LDA) calculations (shown for comparison in Fig. 3). As expected, our low-temperature data are shifted relative to the ambient-temperature data sets, but the error bars on the

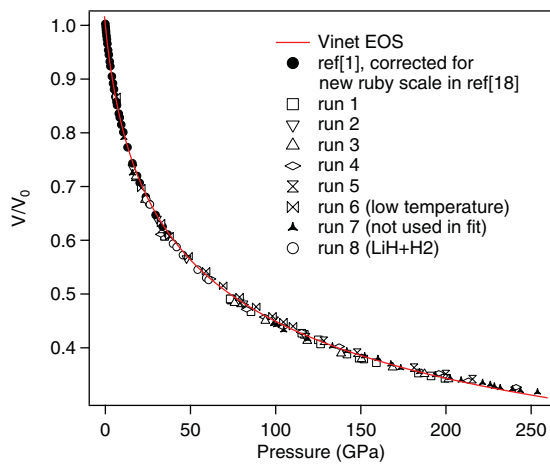


FIG. 4. (Color online) Equation of state of the eight experimental runs, including diffraction from LiH in hydrogen and previous data from Ref. 1. For all data sets except run 6, V_0 is fixed at the best value found in Ref. 1 of 16.9827 \AA^3 . The V_0 value for run 6 was allowed to vary in the equation-of-state fitting procedure, resulting in a value of $16.9(5) \text{ \AA}^3$. Error bars do not exceed the size of the data points.

equation-of-state fitting parameters are sufficiently large due to sparse data that a strong comparison is not possible.

We do not observe evidence for the theoretically predicted $B1$ - $B2$ phase transition at the volume compression predicted ($0.33V_0$). The maximum pressure achieved in our study was within the range of compression at which the transition has been expected, but it is too low to strictly rule out the predictions listed in Table I, with the exception of the Debye-model calculations of Hama *et al.*⁸ However, although

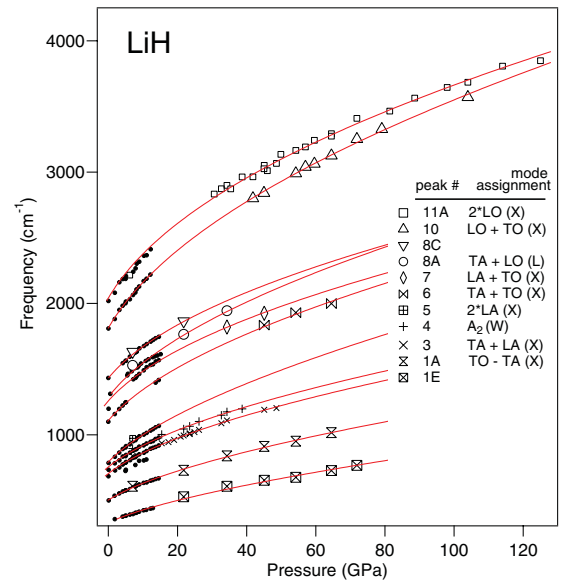


FIG. 5. (Color online) Pressure dependence of two-phonon modes measured from four different samples of LiH, compared with previous results. The modes are assigned following the results of Ho *et al.*³² Solid lines are from curve fits to pressure as a function of frequency, assuming our Vinet equation of state for pressure as a function of volume and a constant Gruneisen model for frequency as a function of volume: $\omega_i = \omega_{0i}(V/V_0)^{-\gamma_i}$. This yields the following functional form: $P = 3B_0(1-x)x^{-2}\exp[\frac{3}{2}(B'_0 - 1)(1-x)]$; $x = (\omega/\omega_0)^{-1/3\gamma}$.

essentially within the error bars for our equation of state, there is some indication of the onset of a departure from a linear trend in the plot of normalized stress vs strain (Fig. 3) above $(1 - X) \sim 0.28$. This effect could signal that the transition is imminent.

Raman mode frequencies under pressure are shown in Fig. 5. Gaps in the data between 1200 and 1500 cm^{-1} and between 2000 and 2700 cm^{-1} result from overlap with the strong first- and second-order Raman features from the diamond anvils. Each peak represents a sum of optical and acoustic modes, and by combining them in various ways, we may extract the pure modes. We calculate the Gruneisen parameters for the longitudinal- and transverse-optical and -acoustic modes by generating the volume dependence of the Raman frequencies from our measured equation of state and fitting the curves with the following expression: $\omega_i = \omega_{0i}(V/V_0)^{-\gamma_i}$. The plot of $\log(\omega_i)$ vs $\log(V/V_0)$ (Fig. 6) will then be linear with a slope equal to the Gruneisen parameter γ_i if γ_i is constant as a function of volume.

The constant Gruneisen approximation appears to be good over this pressure range for the optical modes. For the acoustic modes, LA(X) evolution is clearly deviating from a linear trend, and our data suggest that the TA(X) modes start to deviate as well at high pressure. For the LA(X) mode (following the formation of Ho *et al.*), we assume a volume-dependent-mode Gruneisen parameter,

$$\gamma_i = \gamma_{0i}(V/V_0)^q, \quad (4)$$

yielding the following expression for the frequency:

$$\omega_i = \omega_{0i} \exp\{(\gamma_{0i}/q)[1 - (V/V_0)^q]\}. \quad (5)$$

The data within the region where we see onset of curvature of the TA(X) mode are too sparse to introduce the additional volume-dependent fitting parameter into the fit, so we approximate the trend with a linear fit. Our measured sum modes are in good agreement with those of Ho *et al.*,³² and so we use their data points in our fitting to better constrain the curves at low pressure. The derived-mode Gruneisen parameters and equilibrium frequencies at the X point are shown in Table II

TABLE II. Equilibrium frequencies and mode Gruneisen parameters at the X point compared with previous experimental and theoretical results.

	LO(X)		TO(X)		LA(X)			TA(X)	
	ω_{0i} (cm^{-1})	γ_i	ω_{0i} (cm^{-1})	γ_i	ω_{0i} (cm^{-1})	γ_i	q	ω_{0i} (cm^{-1})	γ_i
Experiments									
This work	1003(3)	0.748(5)	805(3)	0.928(6)	379(5)	1.6(1)	1.4(2)	298(1)	0.78(1)
Ref. 32	1015(6)	0.69(3)	806(2)	0.88(2)	393(1)	1.10(6)	1.4(3)	299.0(8)	0.90(1)
Ref. 33					379			312	
Ref. 34	1054.5		777.5		385			300	
Ref. 35			819					293	
Calculations									
Ref. 32	1408	0.7	793	1.01	443	1.36	1.3	303	0.65
Ref. 36		1.2		1.15		1.88			0.77
Ref. 13	1039		857		457			349	
Ref. 11	1041		821		404			312	
Ref. 34	937		821		392			286	
Ref. 37	944		825		399			291	

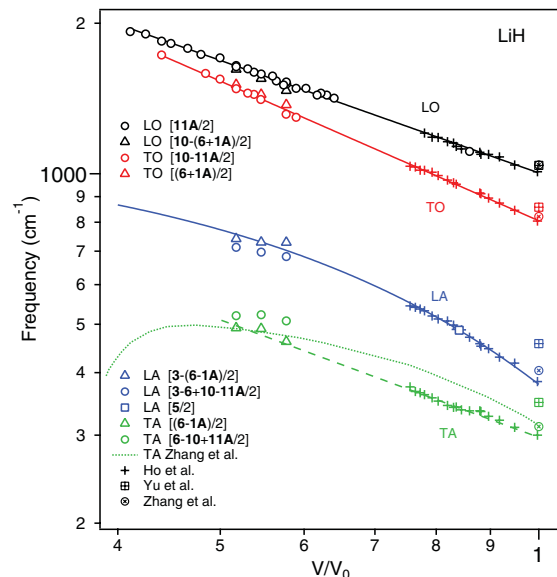


FIG. 6. (Color online) Longitudinal and transverse phonon modes at the X point. Frequencies are calculated from linear combinations of the experimentally observed sum modes (shown in brackets, with peak notations from Fig. 5). The peak 11A assignment is somewhat tentative. This mode was not observed in the experiments of Ho *et al.*, and the LO mode may instead originate from the L , K , or Γ points, which have similar energies. Some theoretically predicted ambient values are shown for comparison (also quoted in Table II). The predicted pressure evolution of the TA mode comes from Zhang *et al.*¹¹ based on a linear response calculation.

and are compared with previous experimental and calculated results.

The calculations of Yu *et al.*¹³ gave the most accurate structural information on LiH, but their predictions for the equilibrium vibrational modes are quite far off. The simpler shell model of Anderson and Lüty³⁴ gives more accurate results, as does the *ab initio* linear-response calculations of Zhang *et al.*,¹¹ which do not include zero-point motion or temperature effects. Zhang *et al.* have also attempted

to predict high-pressure evolution of the TA(X) mode and identify a significant softening at 200 GPa, indicative of a structural instability signaling a phase transition. Our Raman data (although too sparse at high pressure as a result of overlap with diamond Raman) suggest the onset of flattening of the TA curve. As another approach to predicting the $B1$ - $B2$ phase transition, phonon softening is worth further investigation, now that a more complete set of experimental data exists. LiH and LiD have been shown to have very different vibrational spectra,^{13,36} so from the standpoint of understanding the role of quantum effects in LiH, an accurate reproduction of experimental high-pressure trends in phonon frequencies is important. Finally, the splitting of the LO-TO modes is decreasing with density. At the Γ point, the splitting can be directly related to the ionic charge through a simple formula.³⁸ At the X point, the connection is less straightforward and would require extensive calculation beyond the scope of this paper. However, the strong reduction of the LO-TO splitting at the X point could be indicative of a reduction of the ionic character of the compound, which would further explain the change of compressibility observed above 200 GPa.

V. CONCLUSION

Our measurements have yielded a significant amount of structural and vibrational information on the simple system of LiH, from which it becomes evident that a theoretical model has yet to be found that can simultaneously capture the structural and thermodynamic behavior of LiH at high pressure. The long-predicted $B1$ - $B2$ phase transition and accompanying metallization have not been observed up to a 32% volume reduction, but there is some indication in the diffraction and Raman data that it may not be far beyond 252 GPa.

ACKNOWLEDGMENTS

We thank N. W. Ashcroft for useful comments and T. A. Strobel and N. Subramanian for help with the Raman studies. The diffraction was performed on the ID27 beam line at the European Synchrotron Radiation Facility (ESRF), Grenoble, France. The Raman studies were partially supported by NSF-DMR and DOE/NNSA (CDAC).

*lazicki1@llnl.gov

- ¹P. Loubeyre, R. Le Toullec, M. Hanfland, L. Ulivi, F. Datchi, and D. Hausermann, *Phys. Rev. B* **57**, 10403 (1998).
- ²E. Gregoryanz, L. F. Lundegaard, M. I. McMahon, C. Guillaume, R. J. Nelmes, and M. Mezouar, *Science* **320**, 1054 (2008).
- ³C. L. Guillaume, E. Gregoryanz, O. Degtyareva, M. I. McMahon, M. Hanfland, S. Evans, M. Guthrie, S. V. Sinogeikin, and H.-K. Mao, *Nat. Phys.* **7**, 211 (2011).
- ⁴Y. Ma, M. I. Eremets, A. R. Oganov, Y. Xie, I. Trojan, S. Medvedev, A. O. Lyakhov, M. Valle, and V. Prakapenka, *Nature (London)* **458**, 182 (2009).
- ⁵E. Gregoryanz, O. Degtyareva, M. Somayazulu, R. J. Hemley, and H.-K. Mao, *Phys. Rev. Lett.* **94**, 185502 (2005).
- ⁶J. Hammerbert, *J. Phys. Chem. Solids* **39**, 617 (1977).
- ⁷J. Hama and N. Kawakami, *Phys. Lett. A* **126**, 348 (1988).
- ⁸J. Hama, K. Suito, and N. Kawakami, *Phys. Rev. B* **39**, 3351 (1989).
- ⁹J. L. Martins, *Phys. Rev. B* **41**, 7883 (1990).
- ¹⁰G. Roma, C. M. Bertoni, and S. Baroni, *Solid State Commun.* **98**, 203 (1996).
- ¹¹J. Zhang, L. Zhang, T. Cui, Y. Li, Z. He, Y. Ma, and G. Zou, *Phys. Rev. B* **75**, 104115 (2007).
- ¹²S. Lebegue, M. Alouani, B. Arnaud, and W. E. Pickett, *Europhys. Lett.* **63**, 562 (2003).
- ¹³W. Yu, C. Jin, and A. Kohlmeier, *J. Phys. Condens. Matter* **19**, 086209 (2007).
- ¹⁴J. M. McMahon and D. M. Ceperley, *Phys. Rev. Lett.* **106**, 165302 (2011).
- ¹⁵C. L. Guillaume, E. Gregoryanz, O. Degtyareva, M. I. McMahon, M. Hanfland, S. Evans, M. Guthrie, S. V. Sinogeikin, and H.-K. Mao, *Nat. Phys.* **7**, 211 (2010).
- ¹⁶E. Zurek, R. Hoffmann, N. W. Ashcroft, A. R. Oganov, and A. O. Lyakhov, *Proc. Natl. Acad. Sci. USA* **106**, 17640 (2009).
- ¹⁷Y. Kondo and K. Asaumi, *J. Phys. Soc. Jpn.* **57**, 367 (1988).
- ¹⁸J. Y. Zhang, L. J. Zhang, T. Cui, Y. L. Niu, Y. M. Ma, Z. He, and G. T. Zou, *J. Phys. Condens. Matter* **19**, 425218 (2007).

- ¹⁹K. Takemura and A. Dewaele, *Phys. Rev. B* **78**, 104119 (2008).
- ²⁰A. Dewaele, P. Loubeyre, and M. Mezouar, *Phys. Rev. B* **70**, 094112 (2004).
- ²¹A. F. Goncharov, V. V. Struzhkin, R. J. Hemley, H.-K. Mao, and Z. Liu, *Science and Technology of High Pressure*, edited by M. H. Manghnani, W. J. Nellis, and M. Nicol (Universities Press, Hyderabad, India, 2000), pp. 90–95.
- ²²T. S. Duffy, G. Shen, J. Shu, H.-K. Mao, R. J. Hemley, and A. K. Singh, *J. Appl. Phys.* **86**, 6729 (1999).
- ²³A. Kavner and T. S. Duffy, *Phys. Rev. B* **68**, 144101 (2003).
- ²⁴A. K. Singh and K. Takemura, *J. Appl. Phys.* **90**, 3269 (2001).
- ²⁵D. Errandonea, Y. Meng, M. Somayazulu, and D. Häusermann, *Phys. B* **355**, 116 (2005).
- ²⁶Zs. Jenei, H. P. Liermann, H. Cynn, J.-H. P. Klepeis, B. J. Baer, and W. J. Evans, *Phys. Rev. B* **83**, 054101 (2011).
- ²⁷T. S. Duffy, G. Shen, D. L. Heinz, J. Shu, Y. Ma, H.-K. Mao, R. J. Hemley, and A. K. Singh, *Phys. Rev. B* **60**, 15063 (1999).
- ²⁸P. Vinet, J. Ferrante, J. R. Smith, and J. H. Rose, *J. Phys. C* **19**, L467 (1986).
- ²⁹P. Vinet, J. Ferrante, J. H. Rose, and J. R. Smith, *J. Geophys. Res.* **92**, 9319 (1987).
- ³⁰D. R. Stephens and E. M. Lilley, *J. Appl. Phys.* **39**, 177 (1968).
- ³¹D. Gerlich and C. S. Smith, *J. Phys. Chem. Solids* **35**, 1587 (1974).
- ³²A. C. Ho, R. C. Hanson, and A. Chizmeshya, *Phys. Rev. B* **55**, 14818 (1997).
- ³³D. Laplaze, *J. Phys. (Paris)* **37**, 1051 (1976).
- ³⁴A. Anderson and F. Lüty, *Phys. Rev. B* **28**, 3415 (1983).
- ³⁵V. I. Tyutyunnik and O. I. Tyutyunnik, *Phys. Status Solidi B* **162**, 597 (1990).
- ³⁶H. Jex, *J. Phys. Chem. Solids* **35**, 1221 (1974).
- ³⁷Ch. B. Lushchik *et al.*, *Trudy Inst. Fiz. Akad. Nauk Est. SSR* **47**, 7 (1977).
- ³⁸N. W. Ashcroft and N. D. Mermin, *Solid State Physics* (Saunders College, Philadelphia, 1976).